Biophysical Reports

ARTICLE

Proteoliposomes reconstituted with human aquaporin-1 reveal novel single-ion-channel properties

Sam W. Henderson,[1] Yoshitaka Nakayama,[2,6] Murray L. Whitelaw,[3] John B. Bruning,[3] Peter A. Anderson,[4] Stephen D. Tyerman,[5] Sunita A. Ramesh,[4] Boris Martinac,[2,6] and Andrea J. Yool[1,*]

[1]School of Biomedicine, University of Adelaide, Adelaide, SA 5005, Australia; [2]Victor Chang Cardiac Research Institute, Lowy Packer Building, Darlinghurst, NSW 2010, Australia; [3]Institute of Photonics and Advanced Sensing, The School of Biological Sciences, University of Adelaide, Adelaide, SA 5005, Australia; [4]School of Biological Sciences, Faculty of Science and Engineering, Flinders University, Adelaide, SA 5001, Australia; [5]ARC Centre of Excellence in Plant Energy Biology, School of Agriculture, Food and Wine & Waite Research Institute, University of Adelaide, Glen Osmond, SA 5064, Australia; and [6]School of Clinical Medicine, UNSW Medicine & Health, St Vincent's Healthcare Clinical Campus, Faculty of Medicine and Health, University of New South Wales, Sydney, NSW Australia

ABSTRACT Human aquaporin 1 (hAQP1) forms homotetrameric channels that facilitate fluxes of water and small solutes across cell membranes. In addition to water channel activity, hAQP1 displays non-selective monovalent cation-channel activity gated by intracellular cyclic GMP. Dual water and ion-channel activity of hAQP1, thought to regulate cell shape and volume, could offer a target for novel therapeutics relevant to controlling cancer cell invasiveness. This study probed properties of hAQP1 ion channels using proteoliposomes, which, unlike conventional cell-based systems such as *Xenopus laevis* oocytes, are relatively free of background ion channels. Histidine-tagged recombinant hAQP1 protein was synthesized and purified from the methylotrophic yeast, *Pichia pastoris*, and reconstituted into proteoliposomes for biophysical analyses. Osmotic water channel activity confirmed correct folding and channel assembly. Ion-channel activity of hAQP1-Myc-His_6 was recorded by patch-clamp electrophysiology with excised patches. In symmetrical potassium, the hAQP1-Myc-His_6 channels displayed coordinated gating, a single-channel conductance of approximately 75 pS, and multiple subconductance states. Applicability of this method for structure-function analyses was tested using hAQP1-Myc-$His_6^{D48A/D185A}$ channels modified by site-directed mutations of charged Asp residues estimated to be adjacent to the central ion-conducting pore of the tetramer. No differences in conductance were detected between mutant and wild-type constructs, suggesting the open-state conformation could differ substantially from expectations based on crystal structures. Nonetheless, the method pioneered here for AQP1 demonstrates feasibility for future work defining structure-function relationships, screening pharmacological inhibitors, and testing other classes in the broad family of aquaporins for previously undiscovered ion-conducting capabilities.

WHY IT MATTERS A subset of aquaporins (AQPs) conduct monovalent ions. This channel property may contribute to pathogenesis in some human diseases, leading to the proposal that AQPs are promising targets for drug discovery. AQP ion-channel characterization using live cells is often hampered by background ion-channel activity and cell-to-cell variation, which has slowed the progress of discovering new AQP modulators. Here, a cell-free method for recording single human AQP1 (hAQP1) ion channels is presented. Novel features of hAQP1 were identified, including the single-channel conductance and subconductance states in a defined membrane environment. The significance of this method is its potential application to future discovery of new AQP ion-channel blockers, and new classes of ion-conducting AQPs across biological kingdoms.

INTRODUCTION

Aquaporins (AQPs) are multifunctional transmembrane proteins that facilitate the passive movement of water and small solutes across cell membranes. AQPs are permeable to diverse substrates, including water (1,2), glycerol and urea (3–6), hydrogen peroxide (7–9), carbon dioxide (10,11), as well as monovalent anions (12) and cations (13,14). Transcript levels for human AQPs 1–5, 8, and 9 are upregulated in some classes of cancers (15), and these proteins have been proposed as targets for anti-cancer therapies (16,17). AQP mutations cause disorders; for example,

Submitted September 4, 2022, and accepted for publication January 11, 2023.

*Correspondence: andrea.yool@adelaide.edu.au

Editor: Oliver Beckstein.

https://doi.org/10.1016/j.bpr.2023.100100

impaired renal function due to loss of AQP1 function (18) and nephrogenic diabetes insipidus due to mutations in AQP2 (19). SomOther AQP-linked diseases include obesity, congenital cataracts, neuromyelitis optica, and epilepsy (20). New approaches to rapidly characterize diverse AQP activities could facilitate discovery of potential new therapies for AQP-related disorders, as novel compounds could be efficiently screened to determine their AQP-modifying effects (21).

A traditional approach for characterizing AQP activity is heterologous expression using *Xenopus laevis* oocytes (2). This cell type is an excellent model for measuring AQP-facilitated osmotic water permeability (*Pf*) given the oocyte's low endogenous *Pf*. Moreover, oocytes are useful for measuring the whole-cell conductance (G) and single-channel conductance (γ) of heterologously expressed ion channels via two-electrode voltage clamp (TEVC) and patch-clamp recordings respectively (22). Electrophysiological recordings of AQP-expressing oocytes determined that human AQP1 (hAQP1) shows dose-dependent activation by cyclic guanosine monophosphate (cGMP), which activates a non-selective monovalent cation conductance through the central pore (13,23); rat (*Rattus norvegicus*) AQP6 is an anion-permeable channel sensitive to pH and covalent modification by mercuric compounds (12,24), and AtPIP2;1 from *Arabidopsis thaliana* is a calcium-sensitive non-selective cation channel (25,26).

Despite obvious advantages, *Xenopus* oocytes show variable levels of expression of injected channel mRNAs, and activity of endogenous ion channels (27), which can obscure or modify the signals generated by the heterologously expressed channels of interest. The latter was noted for the mammalian voltage-gated potassium (K^+) channel Kv2.1, which showed slower activation in the presence of endogenous oocyte K^+ channels (28). Native oocyte signaling cascades involving kinases and phosphatases can complicate analyses by modulating ion-channel activity, as shown for human KCNQ4 K^+ channels expressed in *Xenopus* oocytes (29) and hAQP1 cation channels (23). Furthermore, seasonal and genetic variations affect *Xenopus* oocyte viability and the efficiency of translation of introduced proteins (30). Collectively, these disadvantages handicap reliability and reduce the consistency of responses needed for mass-throughput screening; for example, in searching for compounds to target AQP ion-channel activity.

An alternative platform for biophysical characterization of AQPs can be achieved by reconstituting purified proteins into lipid vesicles or bilayers. These systems are by design free of background ion channels and intracellular signaling cascades that are present in oocytes and other cell expression systems. Purified bovine MIP26 (BtAQP0) from ocular lens fiber cells, and its orthologs from chicken (MIP28) and soybean (GmNOD26), were characterized as voltage-sensitive anion and/or cation selective channels with large unitary conductances (100–300 pS) in planar lipid bilayers (31–36). Purified native hAQP1 and histidine-tagged recombinant hAQP1 produced using yeast (*Saccharomyces cerevisiae*) both displayed cGMP-activated single-channel sodium (Na^+) and K^+ conductances in planar lipid bilayers (37); however, their unitary conductances were small (not exceeding 10 pS). This contrasted with the large unitary conductance (150 pS) of hAQP1 observed in patch-clamped *Xenopus* oocyte membranes (13). These apparent differences in the single-channel amplitudes of hAQP1 could have arisen due to differences in membrane lipid composition between the preparations (38). Discrepancies in results obtained from different experimental systems is a recognized barrier to progress in aquaporin research (39). Development of rapid, reliable, and reproducible methods for AQP ion-channel characterization in defined membranes will facilitate channel characterization and drug discovery.

Single-channel recordings of recombinant KcsA K^+ channels, and bacterial mechanosensitive ion channels of large (MscL) and small (MscS) conductance, have been successfully recorded using patch-clamp on membrane blisters derived from proteoliposomes (40-42). Blisters are unilamellar bilayers that emerge from the sides of collapsed proteoliposomes in the presence of magnesium (Mg^{2+}) (Fig. 1). This rapid technique has not previously been applied to the characterization of AQP ion-channel proteins. In prior work,

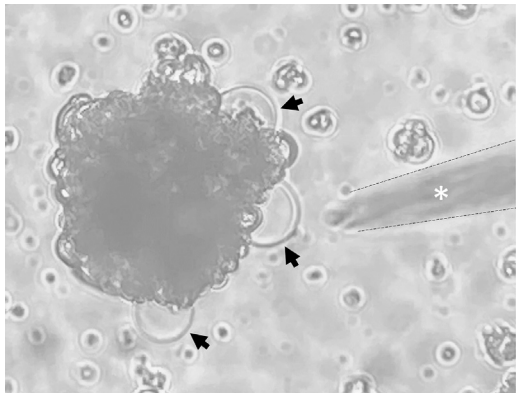

FIGURE 1 Typical unilamellar blisters used for patch-clamp electrophysiology in this study. Phase contrast micrograph of unilamellar membrane blisters (*black arrows*) within solution that have developed from a cluster of collapsed proteoliposomes in the presence of Mg^{2+}. Blisters are amenable to GΩ seal formation with a borosilicate glass micropipette (patch pipette, *white asterisk*). Dashed lines flanking the patch pipette have been added for clarity.

hAPQ1 was produced at high protein densities in heterologous host systems *Pichia pastoris* (43) and *S. cerevisiae* (44). In those studies, hAQP1 retained its correct assembly and function, as demonstrated by the preservation of water channel activity when the proteins were reconstituted into proteoliposomes and measured using stopped-flow spectroscopy in the presence of an osmotic gradient. The capacity for functional recombinant hAQP1 ion channels to be reconstituted into proteoliposomes and detectable using patch-clamp electrophysiology in a defined membrane environment remained a gap in knowledge.

Work here confirmed the feasibility of single-channel patch-clamp analysis of recombinant hAQP1 reconstituted into proteoliposomes and quantified novel properties of the channel. Recombinant hAQP1 with carboxy-terminal Myc and histidine tags (hAQP1-Myc-His_6) was produced at a high purity and concentration from *P. pastoris* as described previously (43) and was demonstrated to be functional with respect to both water and ion-channel activities. Reconstitution of hAQP1-Myc-His_6 into proteoliposomes using a method adapted from Delcour et al. (40) enabled recordings of single channels of large conductance that were attributable to hAQP1. This study paves the way for potentially rapid characterization of novel AQP antagonists as tools for exploring new therapeutic applications and for enabling the discovery of other classes of aquaporins that are capable of functioning as ion channels across the biological kingdoms.

MATERIALS AND METHODS

Construction of *P. pastoris* expression vectors

The *Xenopus* expression vector pXβG-ev1-hAQP1 (2) was used as a template in a PCR reaction to amplify hAQP1. Reactions consisted of plasmid DNA template, 1× Platinum PCR SuperMix High Fidelity (Thermo Fisher) and 200 nM forward and reverse primers containing restriction sites, shown underlined (*Eco*RI forward primer: 5′-CACCGCGGAATTCAAAATGGCCAGCGAGTTCAAG-3′) (*Xba*I reverse primer: 5′-CGCTCTAGAGCTTTGGGCTTCATCTC-3′) (*Apa*I reverse primer: 5′-CGCGGGCCCCTTTGGGCTTCATCTCCAC-3′). The PCR products were directionally cloned into pENTR using the pENTR/D-topo kit (Thermo Fisher). Plasmids were digested with *Eco*RI and either *Xba*I or *Apa*I. The hAQP1 bands were excised from gels, purified using Illustra GFX PCR DNA and Gel Band Purification Kit (GE Healthcare), and ligated into the *Eco*RI and *Apa*I sites of pPICZ-A, or the *Eco*RI and *Xba*I of pPICZ-B, to make translational fusion proteins encoding hAQP1-Myc-His_6-A and hAQP1-Myc-His_6-B.

Constructs (10 μg) were linearized with *SacI*, purified using Illustra GFX PCR DNA and Gel Band Purification Kit, and concentrated by ethanol precipitation. *P. pastoris* strain X33 was transformed with the linearized plasmid by electroporation in a 0.2-cm cuvette using a Micropulser (Bio-Rad) on the "*Pic*" setting. Positive transformants were selected on yeast extract peptone dextrose (YPD) medium containing 1 M sorbitol and 100 μg/mL zeocin. To select for multi-copy insertions, single colonies that appeared after 3 days at 30°C were re-streaked onto YPD containing 500 μg/mL and 1000 μg/mL zeocin and incubated for a further 3 days at 30°C. Transformed clones were validated by colony PCR using the 5′AOX1 primer (5′-GACTGGTTC CAA TTGACAAGC-3′) and gene-specific reverse primer (5′-TCAATG ATGATGATG ATGATGGTC-3′).

A site-directed double-mutant variant of hAQP1-Myc-His_6 (hAQP1-Myc-$His_6^{D48A/D185A}$) was constructed in the pPICZ-B backbone using sequential reactions of the QuikChange II Site-directed mutagenesis kit (Agilent) following manufacturer's procedures. The primers used for round 1 (D48A) were (5′-CACCTTCACGTTGGC CTGGACCGCCGT-3′) and (5′-ACGGCGGTCCAGGCCAACGTGAAGGTG-3′). For round 2 (D185A), the primers were (5′-CCACAGCCAGTGTAGGCAATA GCCA GGAGGT-3′) and (5′-ACCTCCTGGCTATTGCCTACACTGGCTGTGG-3′).

Immunoblotting

Samples diluted in Laemmli sample buffer (62.5 mM Tris-HCl pH 6.8, 10% glycerol, 1% LDS, 0.005% Bromophenol blue, 10% β-mercaptoethanol) (Bio-Rad) were incubated at 65°C for 10 min and loaded onto 12% mini-PROTEAN TGX gels (Bio-Rad). Proteins were electrophoresed at 200 V for 25 min, and then transferred to nitrocellulose membranes (GE Healthcare) in transfer buffer (25 mM Tris, 192 mM glycine, 20% (v/v) methanol) for 1 h at 4°C. Membranes were blocked in TBS-Tween containing 10% skim milk powder, and then probed with rabbit anti-His polyclonal primary antibody (Cell Signaling Technology) (1:1000) overnight at 4°C in 5% skim milk, followed by IRDye 800CW Goat anti-Rabbit secondary antibody (AbCam) (1:5000) for 1 h at room temperature in 5% skim milk. Membranes were imaged using an Odyssey CLx (LI-COR Biosciences).

Production of hAQP1-Myc-His_6

For an initial small-scale screen, seven *P. pastoris* transformants containing pPICZ-A-hAQP1-Myc-His_6 and seven containing pPICZ-B-hAQP1-Myc-His_6 were analyzed. *P. pastoris* were grown overnight in 5 mL of buffered glycerol-complex medium (BMGY) at 30°C with shaking, and then transferred to 5 mL of buffered methanol-complex medium (BMMY) containing 0.5% (v/v) methanol and grown at 30°C with shaking for 24 h. Cells were pelleted and then resuspended in 100 μL of lysis buffer (20 mM Tris-Cl pH 7.6, 100 mM NaCl, 0.5 mM EDTA, 5% (v/v) glycerol, supplemented with 1% aprotinin, 10 μg/mL leupeptin, 10 μg/mL Pepstatin A, 10 mM PMSF, and 2 mM sodium orthovanadate) and 200 μL of 0.5-mm glass beads. Cells were lysed using a Precellys 24 homogenizer (Bertin Instruments) for 3 × 30 s at 4°C. Cell debris was cleared by centrifugation for 500 × *g* for 5 min. Cleared lysates (5 μL) were analyzed by a dot-blot immuno-assay as described previously (45).

A medium-scale screen was performed using single clones containing pPICZ-A-hAQP1-Myc-His_6 and pPICZ-B-hAQP1-Myc-His_6 with confirmed high protein expression levels. Strain X33 harboring BcAP8-His_6 (46) was used as a positive control. *P. pastoris* were grown in 25 mL of BMMY from a starting optical density 600 (OD_{600}) of 1.0. Cells were harvested by centrifugation after 6 h and 24 h. Cells were broken in a 1:1:1 ratio of cells:lyisis buffer:glass beads as described above. Total protein content of the cleared lysate was estimated using the Pierce 660 nm Protein Assay reagent (Thermo Fisher) using bovine serum albumin as a standard. Total protein (10 μg) was mixed with 1× Laemmli buffer and assessed by immunoblotting as described above.

For large-scale production, a single clone of X33/pPICZ-B-hAQP1-Myc-His_6 was grown overnight in BMGY and used to inoculate 4× 1 L of BMMY supplemented with Antifoam 204 (Sigma) and 1% (v/v) methanol to an initial starting OD_{600} of 0.8. Cells were grown at 30°C with vigorous shaking in Thomson Ultra Yield baffled

flasks, and 10 mL of 100% methanol was added after 24 h. Cells were harvested by centrifugation at 5500 × *g* for 15 min after 48 h of growth. Cell pellets were resuspended in an equal volume (v/w) of breaking buffer (20 mM Tris-Cl pH 7.6, 100 mM NaCl, 0.5 mM EDTA, 5% (v/v) glycerol, 1× Complete EDTA-free protease inhibitor cocktail (Roche)) and lysed by six passes through a cell disruptor (Microfluidics M-110L) at 75 psi. The lysate was clarified by centrifugation at 3000 × *g* for 10 min followed by 10,000 × *g* for 30 min at 4°C. To isolate the membrane fraction, the supernatant consisting of the crude extract was centrifuged at 108,000 × *g* for 90 min in a Beckman ultracentrifuge with Type 70 Ti rotor. The membrane pellet was resuspended in 16 mL of breaking buffer (1 mL per 250 mL of starting culture).

Solubilization and purification of hAQP1-Myc-His$_6$

The membrane fraction, comprising 50 mg of total protein, was diluted to 2 mg/mL in solubilization buffer (20 mM Tris-Cl pH 8.0, 100 mM NaCl, 10 mM imidazole, 20% (v/v) glycerol 5% (w/v) octyl β-D-glucopyranoside (β-OG) (Sigma), 1× Complete EDTA-free protease inhibitor cocktail). The mixture was stirred at low speed on ice for 3.5 h. Solubilized protein was cleared by ultracentrifugation at 160,000 × *g* for 30 min at 4°C. The supernatant was incubated overnight at 4°C with 0.6 mL of HisPur Ni-NTA resin (Thermo Fisher), with gentle end-over-end rotation. The mixture was transferred to a 10-mL column (Bio-Rad) and washed with 10 mL of solubilization buffer containing 1% (w/v) β-OG. The protein was then eluted sequentially with 600 μL of solubilization buffer (1% (w/v) β-OG) containing 100, 250, and 475 mM imidazole. Fractions of 200 μL were collected. The total protein content of each fraction was determined, and 1 μg of each fraction was resolved on a TGX gel as described above. The protein bands were visualized using Coomassie staining and imaged on the 700-nm channel of the Odyssey CLx (LI-COR).

Reconstitution of hAQP1-Myc-His$_6$ into proteoliposomes for vesicle shrinkage assays

Small unilamellar vesicles were prepared from *Escherichia coli* Polar Lipid Extract (Avanti). Lipids in chloroform (5 mg) were transferred to a borosilicate glass test tube and dried under a constant stream of N_2 gas, then further dried under vacuum for 45 min. Lipids were rehydrated by vortexing in 500 μL of reconstitution buffer (50 mM Tris-Cl pH 8, 100 mM NaCl) and then sonicated in an ice bath until translucent (about 1 h). The surfactant β-OG was added to a concentration of 1.2% (w/v), and vesicles were incubated for 1 h at room temperature. Protein (100 μg) was added to the liposome suspension, giving a lipid:protein ratio (LPR) of 50:1. After a 20-min incubation at room temperature, the mixture was diluted by adding 17.5 mL of reconstitution buffer and then centrifuged at 140,000 × *g* for 40 min to pellet the proteoliposomes. The proteoliposome pellet was resuspended in reconstitution buffer to a lipid concentration of 2 mg/mL. Control vesicles were prepared in parallel by adding buffer instead of protein.

Reconstitution of hAQP1-Myc-His$_6$ into proteoliposomes for patch-clamp electrophysiology

Two milligrams of azolectin granules (Sigma) were dissolved in 2 mL of chloroform in a clean borosilicate glass test tube. The chloroform was evaporated under a constant stream of N_2 gas with gentle rotation of the tube to obtain a thin lipid film. Chloroform was completely removed from the lipids by further drying in a vacuum desiccator. Lipids were rehydrated with 2 mL of dehydration/rehydration (D/R) buffer (200 mM KCl, 5 mM HEPES pH 7), and then sonicated until opaque. In a clean glass tube, 200 μL of the subsequent liposomes were mixed with recombinant hAQP1-Myc-His$_6$ at a protein:lipid ratio of 1:1000. Volume was increased to 2 mL with D/R buffer and the mixture was incubated for 2 h with gentle rotation. Detergent was removed using Bio-Beads SM-2 Resin (Bio-Rad) following manufacturer's instructions. Detergent-free proteoliposomes were harvested by ultracentrifugation at 217,000 × *g* for 30 min at 4°C and resuspended in 60 μL of D/R buffer. Aliquots of 10 μL were spotted onto clean glass slides and dried in a vacuum desiccator overnight at 4°C.

Stopped-flow spectroscopy

The water transport activity of recombinant hAQP1-Myc-His$_6$-B was assessed by measuring the light scattering on a DX.17MV stopped-flow spectrophotometer (Applied Photophysics, Leatherhead, UK). Within the instrument, control and hAQP1-Myc-His$_6$-containing vesicles were diluted 1:1 with a hyperosmotic buffer (50 mM Tris-Cl pH 8, 100 mM NaCl, 300 mM sorbitol) and 90° light scatter was recorded in volts. Data were normalized, averaged, and presented as the mean of five traces. Rate constants are reported as mean ± 95% confidence interval.

Oocyte expression

The engineered pPICZ-A and -B plasmids were used as templates to amplify hAQP1-Myc-His$_6$-A and hAQP1-Myc-His$_6$-B by PCR using Platinum PCR SuperMix High Fidelity (Thermo Fisher) as described above, with 400 nM of forward 5′-CACCATGGCCAGCGAGTTCAAG-3′ and reverse 5′-TCAATGATGATGATGATGATGGTC-3′ primers. The PCR products were cloned into pENTR (Thermo Fisher) and then subcloned into the *Xenopus* expression vector pGEMHE-DEST using Gateway LR clonase (Thermo Fisher). Expression vectors were linearized with *Nhel*-HF and used to synthesize cRNA encoding hAQP1-Myc-His$_6$-A and hAQP1-Myc-His$_6$-B in an in vitro transcription reaction with the mMessage mMachine T7 kit (Ambion). The cRNA was purified using the MEGAclear Kit (Thermo Fisher), ethanol precipitated, and quantified by agarose gel electrophoresis and UV spectrometry (Nanodrop 2000).

Oocyte swelling assays

Oocytes were injected with 50 nL of water with cRNA encoding hAQP1-Myc-His$_6$ or without RNA (serving as non-AQP-expressing water-injected control oocytes). The amounts of cRNA injected were 1, 2.5, 5, and 10 ng. Oocytes were incubated for 2 days at 18°C in Ringer's solution (96 mM NaCl, 2 mM KCl, 0.6 mM $CaCl_2$, 5 mM $MgCl_2$, 5 mM HEPES pH 7.6, 10% horse serum, 100 U/mL penicillin, 0.1 mg/mL streptomycin, 0.5 mg/mL tetracycline, and 500 μM Na-pyruvate). Water flux rate was assayed by measuring swelling rates in hypotonic saline by videography. Hypotonic saline was made by diluting isosmotic saline with deionized water in a 1:1 ratio.

Electrophysiology

Oocytes were assessed 2 to 3 days post cRNA injection by TEVC using a GeneClamp 500B amplifier (Axon Instruments). Borosilicate glass electrodes were backfilled with 1 M KCl. Currents from oocytes were recorded in Ca^{2+}-free isotonic saline (100 mM NaCl, 2 mM KCl, 5 mM $MgCl_2$, 5 mM HEPES, pH 7.6 NaOH). Conductance was measured in the initial condition, after activation with 10 μM (Rp)-8-(para-chlorophenylthio)guanosine-3′,5′-cyclic monophosphorothioate (CPT)-cGMP (from a 1 mM stock dissolved in Ca^{2+}-free isotonic

saline) and after the addition of 600 μM $CdCl_2$ (from a 60 mM stock) using a voltage step protocol. From a holding potential of −40 mV, command potential was stepped from +60 mV to −120 mV for 200 ms. Data were digitized with a Digidata 1322 (Axon Instruments) and analyzed with pCLAMP Version 8 software (Molecular Devices).

Patch-clamp electrophysiology was performed on proteoliposomes that were rehydrated on glass slides for 1 to 3 days in an equal volume of D/R buffer at 4°C. Rehydrated liposome suspensions (2–4 μL) were added to a patch-clamp recording chamber containing 3 mL of recording buffer (112 mM KCl, 32 mM $MgCl_2$, 4 mM HEPES pH 7, 10 μM CPT-cGMP). Unilamellar blisters formed after approximately 20 min of incubation at room temperature. Pipettes were pulled from borosilicate glass using a vertical puller (Narashige, PP-83) to a resistance of 3 to 5 MΩ in recording buffer. Pipettes were not fire polished or coated and were backfilled with recording buffer without CPT-cGMP. Seals with a resistance greater than 1 GΩ were formed by touching the blister with the electrode, combined with gentle suction. Excised patches (equivalent to the inside-out configuration) were achieved by pulling the pipette away from the blister and briefly exposing the tip to air, then resubmerging. Data were recorded using an Axoclamp 200A amplifier with CV201A headstage (Axon instruments), digitized with a Digidata 1550B (Molecular Devices) with integrated hum silencer, and collected at a sampling frequency of 1 kHz using pCLAMP 11 (Molecular Devices). Single-channel detection and analyses were performed using Clampfit versions 10 and 11 (Molecular Devices). The single-channel search function was used to set channel levels and generate idealized events, from which amplitude histograms were constructed. Events with durations less than 3 ms were excluded. Due to the presence of multiple channels in each patch, the single-channel open probability (P_{open}) could not be accurately quantified using total open time/total time (t_o/T). Instead P_{open} was estimated using $P_{open} = T_o/NT$, where N is the number of channels in the patch, and $T_o = \sum Lt_o$, where L is the level of channel opening. L was set to the highest level observed, which, due to the long gap-free recording times, was estimated to be the best approximation of N. In total, 3.44 h of gap-free data were recorded for empty liposomes, and 15.5 h of gap-free data were recorded for liposomes containing hAQP1. Channels were recorded from two independent preparations of hAQP1-Myc-His_6 protein. AQP1 channels show modal behavior as described previously (13) with long closed or inactive states (lasting many minutes) alternating with equally sustained highly active periods; only recorded sections with at least one active channel were analyzed for the estimated open times presented here.

RESULTS

Carboxyl-terminal tagged hAQP1-Myc-His_6 is a functional water and ion channel when expressed in *X. laevis* oocytes.

hAQP1 was subcloned into the *P. pastoris* pPICZ-A and pPICZ-B expression vectors to produce constructs that differed by two amino acid residues in the linker between the carboxyl (C) terminus of hAQP1 and the Myc tag (Fig. S1). The recombinant C-terminally tagged hAQP1-Myc-His_6 protein from pPICZ-B was shown previously to function as a water channel when reconstituted into proteoliposomes (43); however, the ion conduction properties of hAQP1 with an additional histidine tag were unknown. Therefore, *Xenopus* expression constructs encoding hAQP1-Myc-His_6 from pPICZ-A and pPICZ-B were developed for rapid functional screening. When oocytes were transferred into a 50% hypotonic saline solution, those injected with cRNA encoding for hAQP1-Myc-His_6 from either the -A or -B construct displayed significant increases in cell volume as a function of time due to water influx (Fig. 2 *A*). Non-AQP-expressing control oocytes displayed only a slight increase in volume, indicative of minimal swelling (Fig. 2 *A*). Compared with water-injected control oocytes, the swelling rate was more than ninefold greater for oocytes injected with hAQP1-Myc-His_6, and this difference was statistically significant (Fig. 2 *B*). Immunoblotting of membrane-enriched oocyte fractions with an anti-His antibody detected a band corresponding to the theoretical molecular weight (31.2 kDa) of hAQP1-Myc-His_6, which was absent in non-AQP-expressing water-injected controls (Fig. 2 *C*). This indicated that the increased water permeability of oocytes was due to the presence of hAQP1-Myc-His_6 protein in the oocyte plasma membrane. Oocyte water permeability was positively correlated with the amount of hAQP1-Myc-His_6 cRNA injected (Fig. 2 *D*), a property that has previously been demonstrated for the wild-type AQP1 (2). Hence, hAQP1-Myc-His_6 displayed all the hallmarks of a functional AQP1 water channel when expressed in *Xenopus* oocytes. Water channel function was independent of the *P. pastoris* expression construct from which the tagged AQP1 was derived.

Wild-type AQP1 elicits ion currents in oocytes after stimulation with cGMP (13), which interacts with the gating domain (loop D) at the intracellular side of the protein (23,47,48). To determine whether C-terminal tagging of AQP1 with histidine affected the cGMP-dependent activation of AQP1 ion conductivity, TEVC was performed. Oocytes injected with hAQP1-Myc-His_6 showed an activation of an ion conductance when 10 μM CPT-cGMP was added to the bathing solution, as well as a positive shift in the reversal potential, as would be predicted by the Nernst equation for current mediated by a cation-permeable channel in external 100 mM Na^+ (Fig. 3 *A*). The ionic currents were reduced in the presence of 600 μM $CdCl_2$ (Fig. 3 *A*), consistent with previous findings of Cd^{2+} block of wild-type AQP1 ion channels (26, 49). No currents were activated by cGMP in non-AQP-expressing control oocytes (Fig. 3 *B*). In contrast, control oocytes showed trends toward a slight decrease in conductance after the application of cGMP, also seen with Cd^{2+}. Unlike hAQP1-Myc-His_6, which showed significant activation by cGMP and block by Cd^{2+} (Fig. 3 *C*), slight differences in conductance values for water-injected oocytes were not statistically significant (Fig. 3 *D*). Large whole-cell currents (microamp

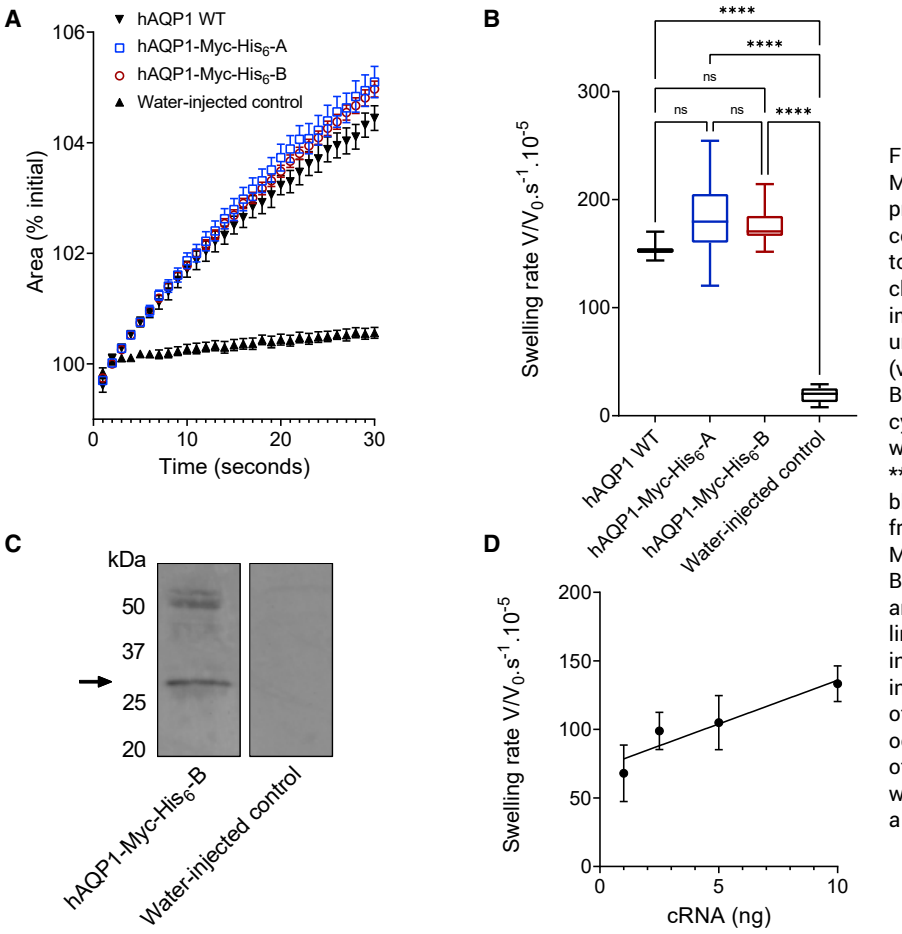

FIGURE 2 Water channel activity of hAQP1-Myc-His_6 in *X. laevis* oocytes. (*A*) Oocytes expressing tagged human hAQP1 variants, or control oocytes, were exposed to 50% hypotonic saline at t = 0. Relative volume change was measured from the time-lapse images. Data are mean ± SEM of three untagged wild-type (WT), 13 (variant A), 12 (variant B), and seven (control) oocytes. (*B*) Boxplots showing the swelling rates of oocytes measured in (*A*). Significant differences were determined by one-way ANOVA. ****$p < 0.0001$; ns, not significant. (*C*) Immunoblot of plasma-membrane-enriched fractions from 15 pooled oocytes injected with hAQP1-Myc-His_6-B or from 15 water-injected controls. Bands were visualized using an anti-His antibody. (*D*) Water permeability increased linearly when oocytes were injected with increasing amounts of cRNA (1–10 ng) encoding hAQP1-Myc-His_6-B. Data are mean ± SD of 10 oocytes (except 2.5 ng, which are 11 oocytes) after the mean water permeability of 12 control oocytes (injected with 50 nL of water) was subtracted. Data were fitted with a linear regression ($R^2 = 0.59$).

amplitude) were elicited by cGMP in hAQP1-Myc-His_6-expressing oocytes (Fig. 3 *E*), consistent with previous results for wild-type AQP1-mediated currents in the oocyte expression system (13). These data show hAQP1-Myc-His_6 is a cyclic nucleotide-gated monovalent cation channel with properties comparable with the wild-type hAQP1 channel when expressed in *Xenopus* oocytes.

Recombinant hAQP1-Myc-His_6 produced in *P. pastoris* forms a functional water channel in proteoliposomes

Quantities of recombinant hAQP1 protein sufficient for crystallization have been synthesized in *P. pastoris* strain X33 using the pPICZ-B expression vector (43). The same approach was used here to produce hAQP1 protein of sufficient quantity and purity for biophysical characterization. The highest-producing transformants were selected from an initial small-scale (5 mL) preparation. After methanol induction of protein expression, crude protein extracts from seven independent transformants were assessed using a protein dot-blot probed with an anti-His antibody (Fig. 4 *A*). Clones from pPICZ-A and pPICZ-B showing the highest expression levels were selected for further work.

A medium-scale study was performed in shake flasks (25 mL) to define the expression levels and induction times for hAQP1-Myc-His_6. Total protein extracts from lysed cells were separated by SDS-PAGE and analyzed by immunoblot with an anti-His antibody. No signal was detected after 6 h (Fig. 4 *B*), which contrasts with a previous study (43). However, after 24 h of induction by methanol, strong signals were observed from protein extracts for two independent transformants (Fig. 4 *B*). Signals could be attributed to hAQP1-Myc-His_6 based on immunoblotting results, which revealed a single band close to 31 kDa that was absent in the untransformed strain X33 (Fig. 4 *B*). The BcAP8 positive control, an aspartic protease from *Botrytis cinerea* that has previously been produced to high densities in *P. pastoris* (46), correctly showed three bands representing the inactive pre-pro-protein, the cleaved active protease, and the smaller pro-domain after cleavage (Fig. 4 *B*). hAQP1-Myc-His_6

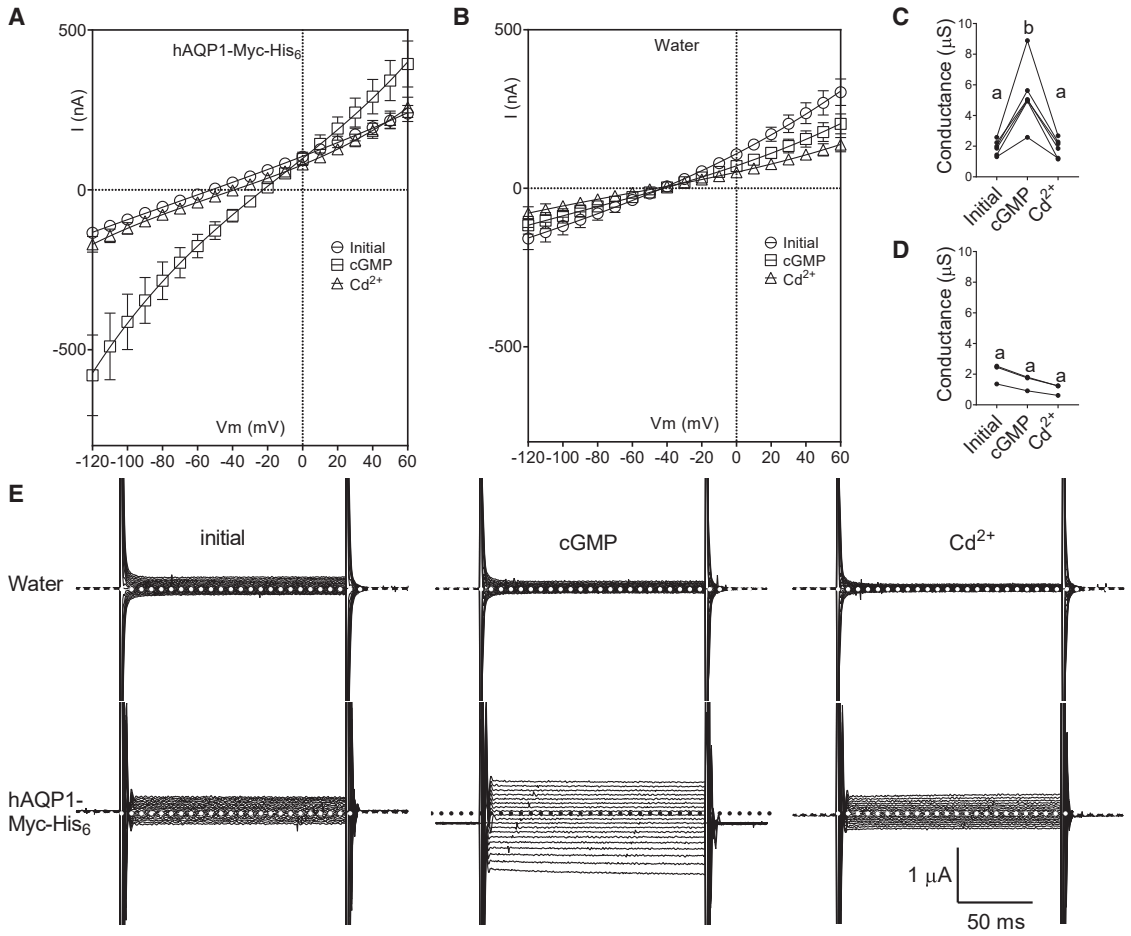

FIGURE 3 Ion-channel activity of hAQP1-Myc-His$_6$ in *X. laevis* oocytes. (*A* and *B*) Current-voltage relationships of oocytes injected with hAQP1-Myc-His$_6$ (*A*) or water-injected controls (*B*) in isotonic Ca^{2+}-free saline at the start of the recording (initial), after activation with 10 μM CPT-cGMP (labeled "cGMP"), and after application of 600 μM $CdCl_2$ to the activated cells (Cd^{2+}). Data are mean ± SEM for six (hAQP1-Myc-His$_6$) or three (water-injected control) oocytes. (*C* and *D*) Slope conductance values for individual oocytes expressing hAQP1-Myc-His$_6$ (*C*) or water-injected controls (*D*) before activation (initial), after activation (cGMP), and after block (Cd^{2+}). Different letters indicate statistically significant differences between the means (ANOVA, $p < 0.001$). (E) Whole-cell current trace recordings illustrate the CPT-cGMP activation of hAQP1-Myc-His$_6$-mediated ion currents. Dashed lines indicate zero current levels.

derived from pPICZ-B produced a stronger signal than that from pPICZ-A (Fig. 4 *B*); the pPICZ-B clone was therefore used to produce recombinant hAQP1-Myc-His$_6$ for biophysical characterization.

Purified hAQP1-Myc-His$_6$ protein was isolated using nickel-NTA agarose affinity chromatography and eluted stepwise from the column by sequentially increasing the concentration of imidazole. Denaturing SDS-PAGE analyses of eight eluate fractions stained with Coomassie blue revealed highly purified samples with major bands representing the hAQP1-Myc-His$_6$ monomer (Fig. 4 *C*). The highest purified protein concentration (up to 4 μg/μL) was achieved in the fractions eluted with 250 mM imidazole. This concentration was sufficient to generate proteoliposomes with protein:lipid ratios suitable for single-channel electrophysiological recordings, as described previously for MscS and MscL (41).

Initially, water channel activity of purified recombinant hAQP1-Myc-His$_6$ was assessed using proteoliposomes. Vesicles were exposed to hypertonic solution in a stopped-flow spectrophotometer, and the rate of vesicle shrinkage was inferred by measuring light scattering as a function of time. The mean response curve of liposomes reconstituted with hAQP1-Myc-His$_6$ displayed robust shrinkage, with a rate constant (k) of 13.3 ± 0.26 s^{-1} (Fig. 4 *D*, blue line). In contrast, empty vesicles without protein showed a slower rate of shrinkage, with a rate constant of 8.9 ± 0.06 s^{-1} (Fig. 4 *D*, gray line). In hAQP1-Myc-His$_6$ vesicles that were incubated with the AQP1 water channel blocker mercuric chloride ($HgCl_2$) (500 μM), the rate constant was reduced to 6.4 ± 0.07 s^{-1}, indicating a reduced rate of vesicle shrinkage (Fig. 4 *D*, red line). These results are consistent with previous findings of hAQP1-Myc-His$_6$ produced in *P. pastoris* and reconstituted

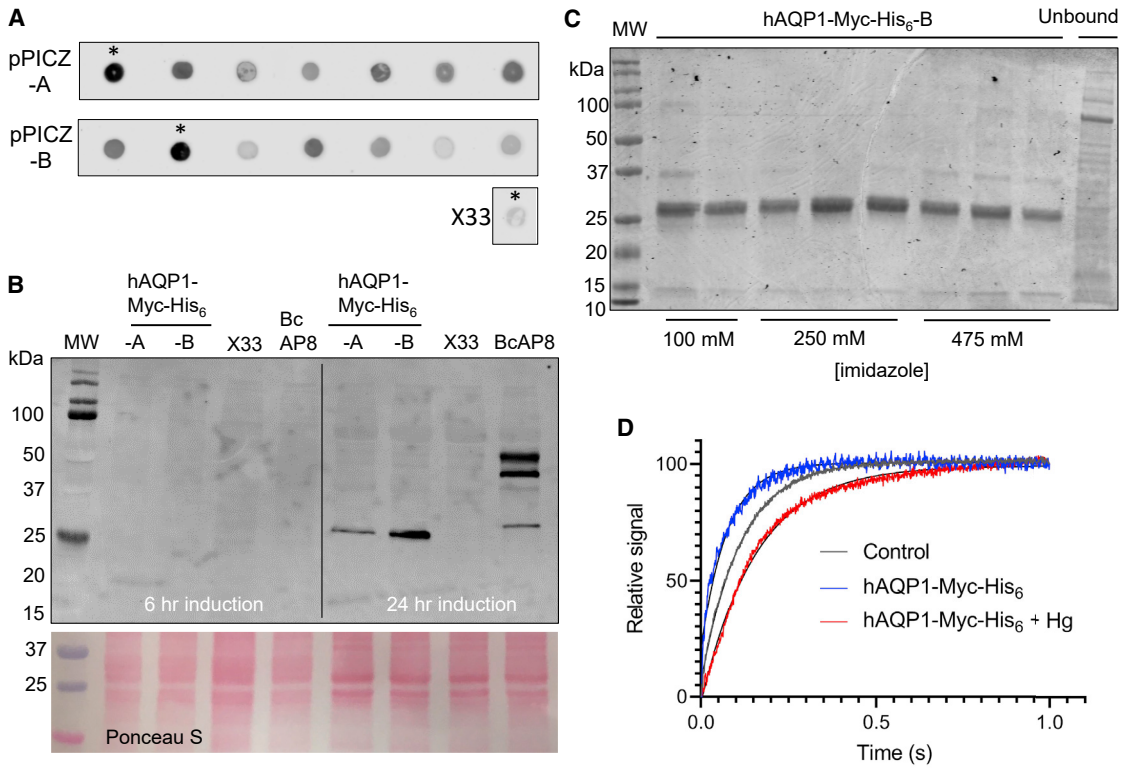

FIGURE 4 Expression and purification of functional recombinant hAQP1-Myc-His_6 water channels from *P. pastoris*. (*A*) Dot-blot screening of crude extracts from independent *P. pastoris* transformants harboring hAQP1-Myc-His_6 from pPICZ-A (*upper*) or pPICZ-B (*lower*). X33 WT control shows low background signal. Asterisks indicates strains used for immunoblot. (*B*) hAQP1-Myc-His_6 detection by immunoblot. *P. pastoris* X33 containing hAQP1-Myc-His_6 from pPICZ-A or -B, untransformed negative control (X33), or BcAP8 (positive control) were induced in BMMY for 6 h (*left*) or 24 h (*right*). Total protein (10 μg) from crude extracts was loaded onto TGX gels, transferred to nitrocellulose, and probed with an anti-His antibody. Total protein loading is demonstrated by Ponceau S staining. (*C*) Coomassie-stained SDS-PAGE gel electrophoresis demonstrates highly purified hAQP1-Myc-His_6 from pPICZ-B. Fractions were eluted from Ni-NTA resin using 100, 250, or 475 mM imidazole. Approximately 1 μg of total protein was loaded per lane. MW, molecular weight marker. (*D*) Stopped-flow spectrometry measurements of water fluxes in proteoliposomes reconstituted with hAQP1-Myc-His_6 (*blue trace*), control liposomes without protein (*gray trace*), and proteoliposomes containing hAQP1-Myc-His_6 that were pre-treated with 500 μM $HgCl_2$ for 20 min (*red trace*). Averages of five traces are shown as colored lines and represent the light scatter of vesicles. Fitted exponential curves are shown as black lines.

into proteoliposomes (43), and indicated that the functional protein had been synthesized and assembled correctly, confirming the channel integrity needed for subsequent biophysical investigations of ion-channel function performed using electrophysiology.

Patch-clamp recordings of reconstituted hAQP1-Myc-His_6 channels in liposomes reveals cGMP-activated K^+ channel activity

The electrical activity of channels in proteoliposomes was assessed using patch-clamp electrophysiology of excised inside-out patches from unilamellar membrane blisters. When patches containing hAQP1-Myc-His_6 were held at a constant voltage of −100 mV, the application of 10 μM CPT-cGMP (labeled in the figure as "cGMP") to the bath triggered a flickering conductance activity and included events seen as long bursts of channel openings interrupted by brief closings (Fig. 5 *A* and *B*). The amplitudes of the channel opening events showed apparent stepwise transitions to amplitudes greater than 60 pA, indicating that the single-channel conductance was high or that multiple channels could be gated cooperatively to account for the observed activity (Fig. 5 *B*). In contrast, control patches from empty liposomes without added AQP1 protein ($n = 18$) did not display channel activity (Fig. 5 *C* (+60 mV) & 6C (±100 mV)) with or without CPT-cGMP. Electrical noise was occasionally observed in patches due to poor seal formation, but this was clearly distinguishable from ion-channel activity. The orientation of hAQP1-Myc-His_6 within the membrane patches was unknown, but it was likely to be a random mixture of cytoplasmic-side-out and extracellular-side-out configurations.

Single channels were observed in some patches (Fig. 6). No net current was observed when the membrane was clamped at 0 mV, as expected for a cation channel in symmetrical K^+ solutions (Fig. 6 *A*). Channel activity detected over a broad range of membrane

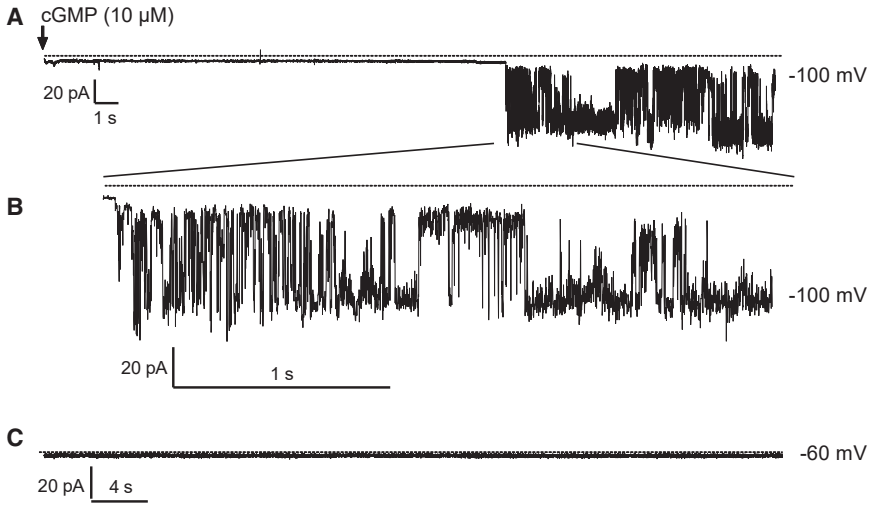

FIGURE 5 cGMP-stimulated electrical properties of proteoliposomes reconstituted with hAQP1-Myc-His_6. (*A*) Gap-free recording of an inside-out patch from a proteoliposome containing hAQP1-Myc-His_6 in symmetrical (112 mM) K^+ solutions at −100 mV. Arrow indicates time of CPT-cGMP addition (labeled "cGMP"). (B) Increased-resolution view of (*A*). (*C*) Gap-free recording of a control (empty) proteoliposome at −60 mV in the presence of 10 μM CPT-cGMP. Dotted lines indicate zero current levels.

potentials showed no apparent voltage dependence (Fig. 6 *B*). Once channels were activated, the predominant pattern was that multiple channels remained open for long durations; thus, fully closed states representing the zero-current baseline were rare. In patches in which apparent single-channel events were detected, the estimated open probability was close to 1 at all tested voltages (Fig. 6 *B*). This is likely to be due to the presence of cGMP in the bath, which has been shown to increase the open probability of AQP1 channels in oocyte membranes (13). Hence the open probability of AQP1 channels was close to 1, as they were recorded in their open states. Channel activity was absent in control patches (Fig. 6 *C*). Single-channel amplitude histograms were constructed from events measured at different holding potentials and fitted with Gaussian functions to determine mean single-channel current amplitudes. An example compiled for events at −100 mV is shown in Fig. 6 *D*. For purposes of calculating channel event amplitudes, the detection algorithm baseline was set at the highest conductance state (the maximum number of open channels), and single-channel amplitudes were quantified from the step changes during closing event deflections (Fig. 6 *B*). Single-channel conductances were determined from linear fits of current-voltage (I/V) plots, from three patches from different proteoliposomes (Fig. 6 *E*). The recombinant hAQP1-Myc-His_6 showed a mean single-channel conductance (γ) of 75.4 ± 7.2 pS (SD).

The amplitude histograms revealed subconductance states (Fig. 6 *D*) that were more apparent when the holding potential was clamped at supraphysiological voltages (exceeding ±100 mV). For example, at +200 mV, hAQP1-Myc-His_6 events showed predominant residence times at an amplitude near 16 pA. Intermittently, a subconductance state of 5 pA was combined (Fig. 7 *A*), reaching an amplitude near 21 pA for the apparent open channel amplitude (Fig. 7 *B*). This small excursion could suggest that open channels can transition occasionally to a slightly higher conducting state, or that an additional channel in the population operating at a small subconductance amplitude contributes to the activity, but with a relatively low open probability.

To further assess the utility of the reconstituted proteoliposome method for AQP analyses, a double-mutant construct of hAQP1, replacing two aspartate (D) residues with alanine (A), was constructed (Fig. 8 *A*). We attempted to produce four different mutant variants of hAQP1 (hAQP1$^{D48K/D185K}$, hAQP1$^{D48N/D185N}$, hAQP1$^{D48R/D185R}$, and hAQP1$^{D48A/D185A}$). However, in this project, only the hAQP1$^{D48A/D185A}$ double mutant produced sufficient protein yields for reconstitution, whereas the other mutants did not. The rationale was based on AQP1 crystal structure; a ring of Asp is shown to surround the central pore (Fig. 8 *A*), and might influence ion permeation (50), resulting in an altered single-channel conductance. A disadvantage of this approach is that available crystal structures for AQP1 have been generated in the absence of a stimulus (cGMP ligand), and thus are likely to represent a closed/non-activated ion-channel state. Similar to the wild type, the mutant construct hAQP1-Myc-$His_6^{D48A/D185A}$ showed ion-channel activity that was activated by CPT-cGMP in *Xenopus* oocytes (Fig. 8 *B*). With patch-clamp, single-channel activity of the mutant construct was demonstrated, but no difference between hAQP1-Myc-His_6 and hAQP1-Myc-$His_6^{D48A/D185A}$ in single-channel conductance was observed (Fig. 8 *C* and *D*).

DISCUSSION

First described as the channel-forming integral membrane protein of 28 kDa (CHIP28), hAQP1 was shown

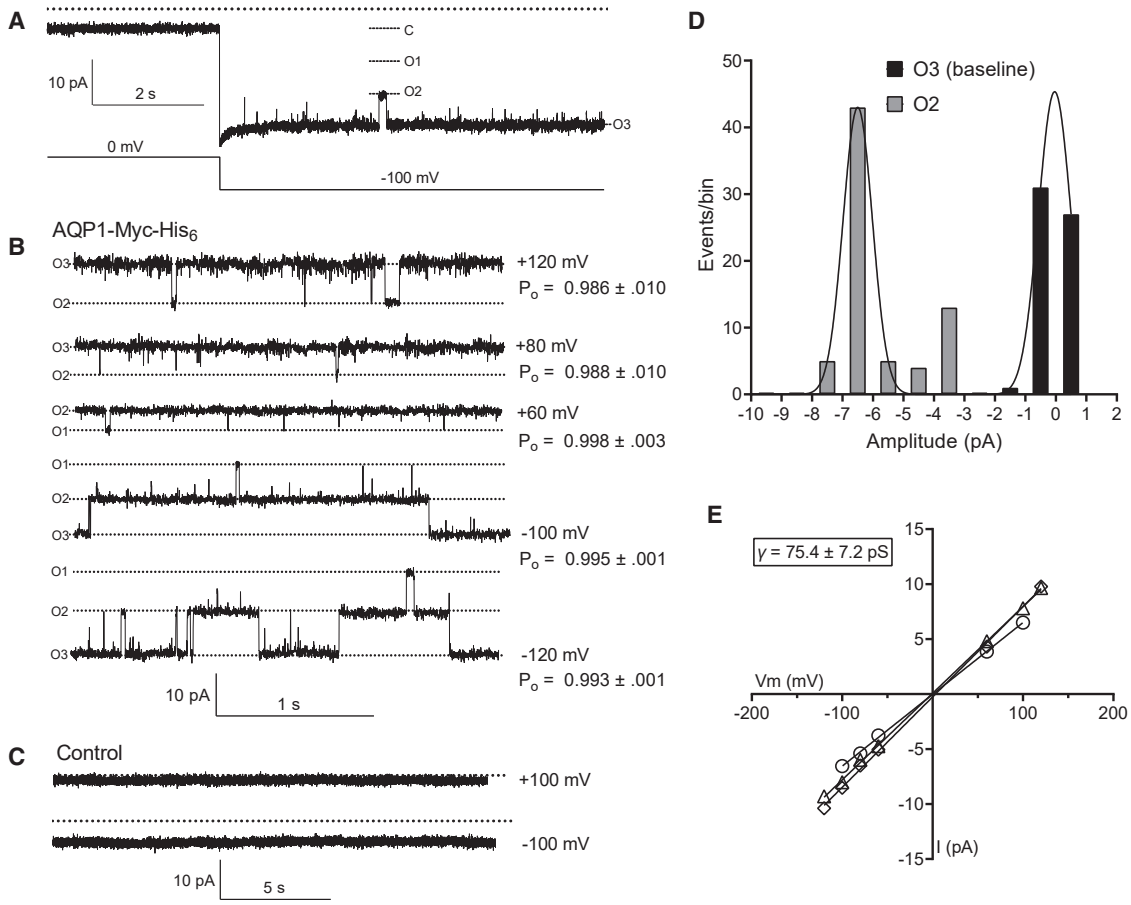

FIGURE 6 Single-channel properties of hAQP1-Myc-His$_6$ in patch-clamped proteoliposomes. (*A*) Gap-free recording of an inside-out patch from a proteoliposome containing hAQP1-Myc-His$_6$ in symmetrical (112 mM) K^+ solutions at 0 and −100 mV (shown below the trace). Dotted line indicates zero current level; dashed lines denote channel configurations where C is closed and O is open. (*B*) Single-channel bursts of hAQP1-Myc-His$_6$ activity recorded during steps to different holding potentials (indicated at the right of each trace) for 2.7 s (total). Dashed lines indicate different open-state levels. Open probability (P_o) ± SD is shown for each voltage. P_o analyses were done specifically on recorded segments that had active channels. (*C*) Recordings of control patches from liposomes without hAQP1-Myc-His$_6$ at ±100 mV showed no single-channel activity. Dotted lines indicate zero current levels. (*D*) Amplitude histogram of idealized events at −100 mV fitted with a Gaussian function that indicates two open-state levels and a single-channel amplitude of 6.5 pA (± 0.48 SD). (*E*) Current-voltage relationships of hAQP1-Myc-His$_6$ in symmetrical (112 mM) K^+ solutions. Unitary amplitudes were plotted against pipette voltage (× −1) for three independent inside-out patches, as shown with different symbols. The mean unitary conductance (*γ*) ± SD (see inset), was determined from the slope of the linear regression line fits.

to facilitate transmembrane water fluxes in *Xenopus* oocytes (2) and reconstituted in proteoliposomes (51). Later work demonstrated that hAQP1 expressed in *Xenopus* oocytes mediated a gated cation-channel activity (52) with a single-channel conductance of 150 pS, activated by cGMP (13). Although the ion-channel property of hAQP1 was initially questioned (53), similar results were obtained for rat AQP1 natively expressed in choroid plexus (49). Ion-channel activity was verified independently in a study showing hAQP1 reconstituted into planar lipid bilayers exhibited cGMP-dependent cation-channel activity, albeit at a low unitary conductance, 10 pS in 100 mM Na^+ or K^+ (37). Work here with proteoliposomes containing recombinant hAQP1-Myc-His$_6$ showed the unitary conductance of hAQP1 is greater when reconstituted in a membrane lipid environment; azolectin-based proteoliposomes showed channel events with a conductance near 75 pS in 112 mM symmetrical KCl saline. The appearance of additional subconductance states could offer insight into discrepancies observed between experimental preparations.

The unitary conductance of hAQP1 in proteoliposomes (75 pS) is approximately half that measured in excised patches from *Xenopus* oocytes (150 pS) (13) but more than sevenfold greater than seen in lipid bilayers. Henderson and colleagues (38) have proposed the variations could reflect differences in membrane compositions of *Xenopus* oocytes compared with planar bilayers (37) or the soybean phospholipid

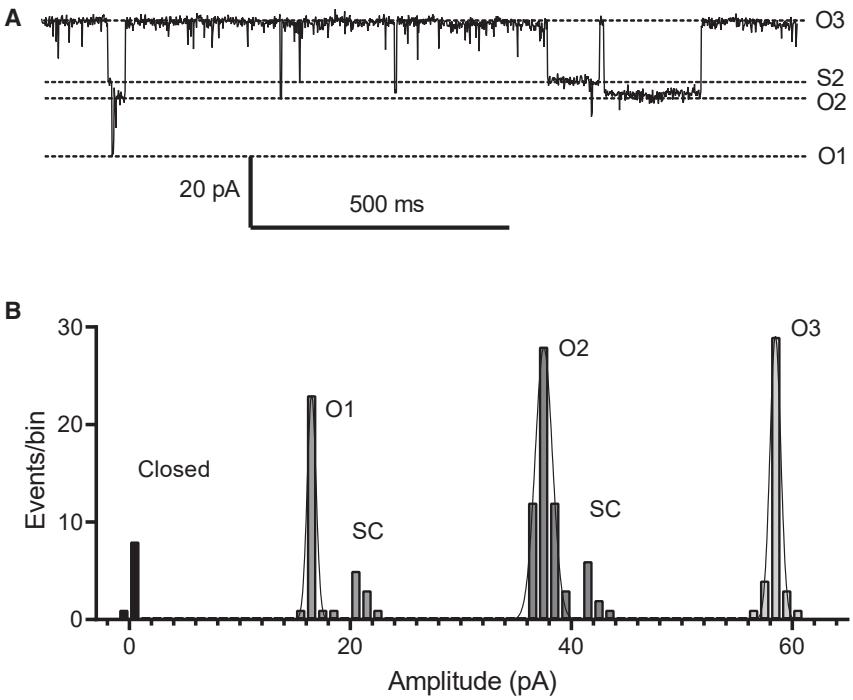

FIGURE 7 hAQP1-Myc-His_6 displays subconductance states. (*A*) Gap-free recording of an inside-out patch from a proteoliposome containing hAQP1-Myc-His_6 in symmetrical (112 mM) K^+ solutions at +200 mV with 10 μM CPT-cGMP. Dashed lines show the different channel conductance levels; O is open and S is subconductance. (*B*) Amplitude histogram of data in (*A*) fitted with Gaussians at open (O) levels 1, 2, and 3. SC, subconductance.

mixture (azolectin) used in this study. Other work has shown that the water permeability of bovine lens aquaporin BtAQP0 was reduced when reconstituted in proteoliposomes with high cholesterol or sphingomyelin (54); similarly, AQPZ from *E. coli* displayed higher water permeability when reconstituted into liposomes made from 1,2-dioleoyl-sn-glycero-3-phosphocholine (DOPC) compared with 1,2-dioleoyl-sn-glycero-3-phosphoglycerol (DOPG) (55). Given that the functional properties of other ion channels (e.g., K^+ channels and ligand-gated nicotinoid receptors) are sensitive to lipid environments (56,57), it is reasonable to speculate that hAQP1 ion channels are affected by membrane composition. Future work using methods described in this study would be of interest to ascertain the modulatory effects of membrane lipids on hAQP1 ion-channel activity.

The maximum conductance measured for hAQP1-Myc-His_6 in proteoliposomes was 75 pS, and a small subconductance state (5 pS) also was detected (Fig. 7). An interesting explanation for the lower hAQP1 conductance values (2, 6, and 10 pS) reported in planar lipid bilayers (37) might be that the bilayer preparation favored the hAQP1 subconductance states, possibly as a result of differences in membrane lipid composition or other factors that remain to be identified. Homologous ion-conducting AQPs from animals (bovine, BtAQP0) (31) and plants (soybean, GmNOD26) (35) showed subconductance state activity when reconstituted in planar lipid bilayers. Multiple conductance states are a widespread feature of many types of ion channels, seen in diverse classes ranging from cardiac sodium channels (58) to non-selective cation channel Polycystin-2 (59) and cyclic nucleotide-gated channels, in which the probability of occupying subconductance states depends in part on the number of cGMP ligands bound to the protein (60). Future work investigating factors that influence hAQP1 occupancy of subconductance states might consider dose-dependent effects of cGMP concentration, block by divalent cations, or contributions of residues lining the central pore, which is the proposed ion conduction pathway in hAQP1 tetramers (Fig. 8A) (48). Future work might also explore the channel properties of recombinant AQPs synthesized from different host cells, including insect (61), yeast (44), and mammalian cell lines (62), which could give rise to a clearer understanding of the effects of posttranslational modifications on hAQP1 function.

The AQP superfamily extends across all kingdoms of life, although only a subset of this broad channel family has thus far been found to conduct monovalent ions (38,63,64). It is likely many as-yet unknown ion-conducting AQPs remain to be discovered. Not all AQPs reside within plasma membranes that are accessible to patch-clamp electrophysiology. For example, AQP11 is localized to the endoplasmic reticulum (65), and AQP12 similarly has been suggested to be localized to intracellular organelles (66). Reconstitution of these recombinant AQPs into membrane blisters could potentially elucidate novel AQP ion-channel functionalities. As-yet uncharacterized AQPs such as

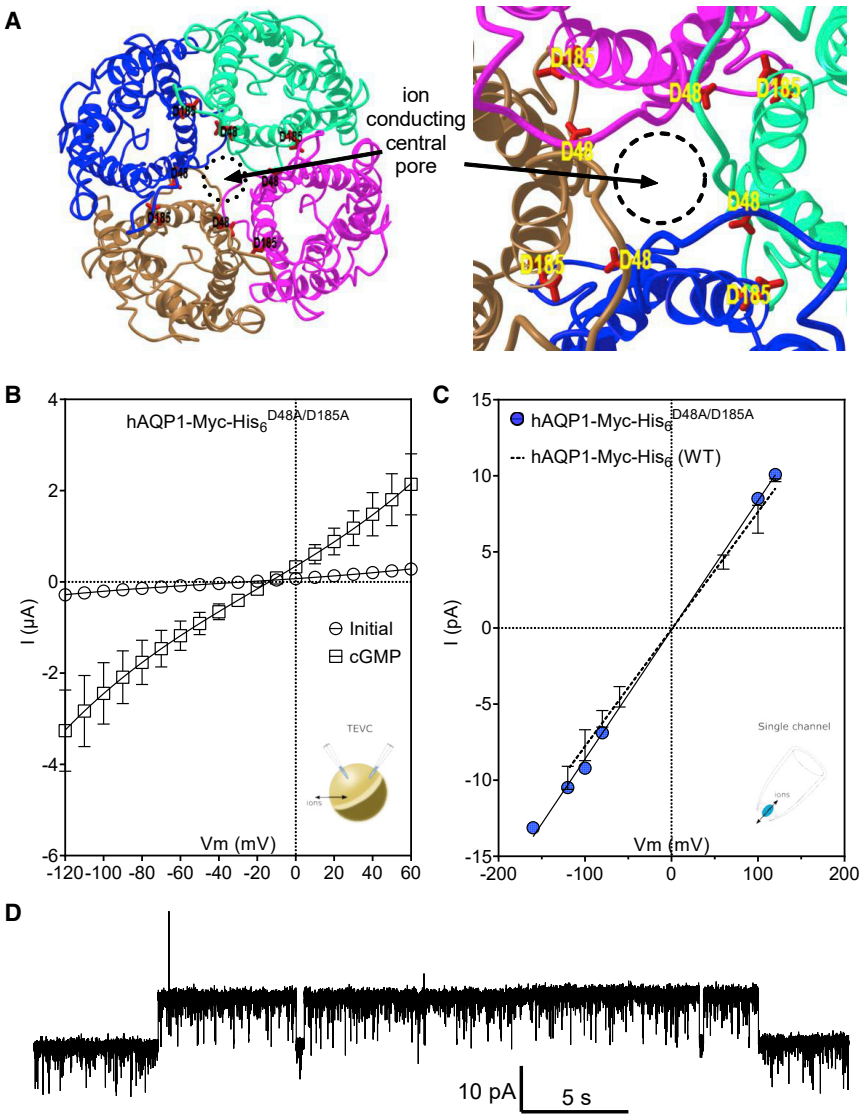

FIGURE 8 Application of the patch-clamp method to investigate a double-mutant variant hAQP1-Myc-$His_6^{D48A/D185A}$ in proteoliposomes. (*A*) Structural view of hAQP1 homotetramer (PDB: 1IH5) displaying a ring of charged Asp (D) residues (*red*) near the ion-conducting central pore, generated using the National Center for Biotechnology Information interactive iCN3D viewer (https://www.ncbi.nlm.nih.gov/Structure). Left, full view; right, higher-magnification inset. (*B*) Current-voltage relationships of oocytes injected with hAQP1-Myc-$His_6^{D48A/D185A}$ in isotonic Ca^{2+}-free saline (initial), and after activation with 10 μM CPT-cGMP. Data are mean ± SEM of six oocytes. (*C*) Current-voltage relationship of purified hAQP1-Myc-$His_6^{D48A/D185A}$ in symmetrical (112 mM) K^+ solutions in a single inside-out proteoliposome patch (*blue circles*). Data for WT hAQP1-Myc-His_6 with error bars (SD) are displayed for comparison (*dashed line*). (*D*) Example of a gap-free recording of an inside-out patch from a proteoliposome containing hAQP1-Myc-$His_6^{D48A/D185A}$ in symmetrical (112 mM) K^+ solutions at 120 mV with CPT-cGMP displaying channel activity.

plant X intrinsic proteins (XIPs), which have been proposed as candidate ion-conducting AQPs (64), could be capably assessed using the techniques described in this study.

AQPs are implicated in a range of human diseases and have attracted interest as potential therapeutic targets. Human AQP1 and AQP4, for example, are strongly elevated in glioblastoma cells (17). AQP1 has been proposed to facilitate glioblastoma invasiveness via a mechanism that is dependent on both its water and cation influx activities (67). Combined inhibition of hAQP1 ion and water channel pores was shown to slow colon cancer cell migration in vitro more effectively than blocking single AQP1 permeation pathways alone (68). The cation conductance of hAQP1 was proposed to account for a hypoxia-induced ionic leak current in sickled erythrocytes that was blocked by the anti-sickling compound 5-hydroxylmethyl-2-furfural and structurally related furan compounds (69). The discovery of new medicinal compounds that regulate AQP ion channels has clear potential to expand therapeutic options, a goal that would benefit from establishment of a rapid screening technique free from background interference. A high-throughput electrophysiological evaluation using reconstituted AQP1 proteoliposomes could expedite discovery of AQP-inhibiting pharmacological agents.

Caveats of the patch-clamp approach for assessing hAQP1-Myc-His_6 activity in proteoliposomes should be noted. Despite the apparent simplicity of the method, the percentage of excised patches containing discernible channel activity was 40%, ($n = 53$ patches), and patches harboring single ion channels were rare. In another study, green fluorescent protein (GFP)-tagged Transmembrane Channel Like (TMC) proteins

1 and 2 were successfully analyzed in proteoliposomes using the patch-clamp (70). Therefore, the efficiency of detecting hAQP1 single channels may be improved by reconstituting liposomes with a fluorescent fusion protein (hAQP1-GFP) to visually identify blisters containing hAQP1, provided that tagging does not modify the ion conductance properties. Second, although relatively pure and biologically active hAQP1-Myc-His_6 was produced, the effects of long-term storage on protein activity were not assessed. The orientations of the channels in the proteoliposome membranes were unknown, which could have implications for mechanistic understanding of the channel. Further purification of hAQP1-Myc-His_6 might improve the long-term reproducibility of patch-clamping proteoliposomes reconstituted with the protein as an efficient and viable alternative to cell-based systems for compound screening.

An example of the application of the method was demonstrated by investigating the functional properties of hAQP1-Myc-$His_6^{D48A/D185A}$. The mutant protein displayed cGMP-activated cation-channel activity in *Xenopus* oocytes but showed no apparent difference in single-channel amplitude. The negatively charged Asp residues might not be located sufficiently close to the central ion-conducting pore in the open state to influence cation permeation. Alternatively, anions might carry electroneutral currents in the mutant channel. It also is conceivable that the conformation of the open AQP1 channels could be quite different from closed-state views that have been deduced from crystal structural analyses, suggesting better identification of pore lining residues might await new methods for crystallizing the channel in a constitutively ion-channel-activated state. The potential impact of introduced mutations on protein production, as we noted when only one of four tested double-mutant constructs was successfully reconstituted, might be noted with interest in future studies. Charged residues (such as D48 and D185 tested here) could affect structural properties influencing reconstitution, beyond possible effects on channel conductance alone. Nonetheless, successful reconstitution and characterization of the mutant AQP1 construct demonstrates that testing of channel properties by mutagenesis is feasible, and could provide in-depth understanding of mechanisms of ionic selectivity, open probability, cooperativity, and open dwell times that are not measurable using TEVC.

In summary, hAQP1-Myc-His_6 ion channels were characterized here using patch-clamp in a clean, molecularly defined system, establishing a new tool for assessing aquaporin ion-channel function in a preparation in which interference from background proteins is minimized. Establishing this assay paves the way for future work identifying new classes of ion-conducting AQPs and screening for AQP ion-channel inhibitors that could have valuable therapeutic uses.

SUPPORTING MATERIAL

Supporting Material can be found online at https://doi.org/10.1016/j.bpr.2023.100100.

AUTHOR CONTRIBUTIONS

A.J.Y., S.A.R., S.D.T., and S.W.H. conceived and designed the analysis. S.W.H., Y.N., B.M., S.D.T., and A.J.Y. collected the data. P.A.A., M.W., and J.B.B. contributed data or analysis tools. S.W.H. performed the analysis. S.W.H. and A.J.Y. wrote the paper. All authors reviewed and approved the final manuscript.

ACKNOWLEDGMENTS

This work was funded by the Medical Advances Without Animals Trust grant to S.W.H., A.J.Y., and B.M.; and the Australian Research Council (ARC) grant DP190101745 to A.J.Y. and S.A.R. Further support was provided from the National Health and Medical Research Council of Australia for a Principal Research Fellowship (APP1135974) to B.M.

DECLARATION OF INTERESTS

The authors declare no competing interests.

REFERENCES

1. Day, R. E., P. Kitchen, …, M. T. Conner. 2014. Human aquaporins: Regulators of transcellular water flow. *Biochim. Biophys. Acta Gen. Subj.* 1840:1492–1506. https://doi.org/10.1016/j.bbagen.2013.09.033.
2. Preston, G. M., T. P. Carroll, …, P. Agre. 1992. Appearance of water channels in *Xenopus* oocytes expressing red cell CHIP28 protein. *Science.* 256:385–387. https://doi.org/10.1126/science.256.5055.385.
3. Ishibashi, K., S. Sasaki, …, T. Gojobori. 1994. Molecular cloning and expression of a member of the aquaporin family with permeability to glycerol and urea in addition to water expressed at the basolate ral membrane of kidney collecting duct cells. *Proc. Natl. Acad. Sci. USA.* 91:6269–6273. https://doi.org/10.1073/pnas.91.14.6269.
4. Liu, Y., D. Promeneur, …, J. M. Carbrey. 2007. Aquaporin 9 is the major pathway for glycerol uptake by mouse erythrocytes, with implications for malarial virulence. *Proc. Natl. Acad. Sci. USA.* 104:12560–12564. https://doi.org/10.1073/pnas.0705313104.
5. Meinild, A.-K., D. A. Klaerke, and T. Zeuthen. 1998. Bidirectional water fluxes and specificity for small hydrophilic molecules in aquaporins 0–5. *J. Biol. Chem.* 273:32446–32451. https://doi.org/10.1074/jbc.273.49.32446.
6. Gotfryd, K., A. F. Mósca, …, P. Gourdon. 2018. Human adipose glycerol flux is regulated by a pH gate in AQP10. *Nat. Commun.* 9:4749. https://doi.org/10.1038/s41467-018-07176-z.
7. Bienert, G. P., A. L. Møller, …, T. P. Jahn. 2007. Specific aquaporins facilitate the diffusion of hydrogen peroxide across

membranes. *J. Biol. Chem.* 282:1183–1192. https://doi.org/10.1074/jbc.M603761200.

8. Miller, E. W., B. C. Dickinson, and C. J. Chang. 2010. Aquaporin-3 mediates hydrogen peroxide uptake to regulate downstream intracellular signaling. *Proc. Natl. Acad. Sci. USA.* 107:15681–15686. https://doi.org/10.1073/pnas.1005776107.
9. Hara-Chikuma, M., H. Satooka, …, A. S. Verkman. 2015. Aquaporin-3-mediated hydro gen peroxide transport is required for NF-κB signalling in keratinocytes and development of pso riasis. *Nat. Commun.* 6:7454. https://doi.org/10.1038/ncomms8454.
10. Endeward, V., R. Musa-Aziz, …, G. Gros. 2006. Evidence that aquaporin 1 is a major pathway for CO_2 transport across the human erythrocyte membrane. *Faseb. J.* 20:1974–1981. https://doi.org/10.1096/fj.04-3300com.
11. Nakhoul, N. L., B. A. Davis, …, W. F. Boron. 1998. Effect of expressing the water channel aquaporin-1 on the CO2 permeability of Xe nopus oocytes. *Am J. Physiol.* 274:C543–C548. https://doi.org/10.1152/ajpcell.1998.274.2.C543.
12. Yasui, M., A. Hazama, …, P. Agre. 1999. Rapid gating and anion permeability of an intracellular aquaporin. *Nature.* 402:184–187. https://doi.org/10.1038/46045.
13. Anthony, T. L., H. L. Brooks, …, A. J. Yool. 2000. Cloned human aquaporin-1 is a cyclic GMP-gated ion channel. *Mol. Pharmacol.* 57:576–588. https://doi.org/10.1124/mol.57.3.576.
14. Yool, A. J., and E. M. Campbell. 2012. Structure, function and translational relevance of aquaporin dual water and ion channels. *Mol. Aspect. Med.* 33:553–561. https://doi.org/10.1016/j.mam.2012.02.001.
15. De Ieso, M. L., and A. J. Yool. 2018. Mechanisms of aquaporin-facilitated cancer invasion and metastasis. *Front. Chem.* 6. https://doi.org/10.3389/fchem.2018.00135.
16. Verkman, A. S., M. O. Anderson, and M. C. Papadopoulos. 2014. Aquaporins: important but elusive drug targets. *Nat. Rev. Drug Discov.* 13:259–277. https://doi.org/10.1038/nrd4226.
17. Yool, A. J., and S. Ramesh. 2020. Molecular targets for combined therapeutic strategies to limit glioblastoma cell migration and invasion. *Front. Pharmacol.* 11. https://doi.org/10.3389/fphar.2020.00358.
18. King, L. S., M. Choi, …, P. Agre. 2001. Defective urinary concentrating ability due to a complete deficiency of aquaporin-1. *N. Engl. J. Med.* 345:175–179. https://doi.org/10.1056/nejm200107193450304.
19. Sands, J. M., and J. D. Klein. 2016. Physiological insights into novel therapies for nephrogenic diabetes insi pidus. *Am. J. Physiol. Ren. Physiol.* 311:F1149–F1152. https://doi.org/10.1152/ajprenal.00418.2016.
20. Verkman, A. S. 2012. Aquaporins in clinical medicine. *Annu. Rev. Med.* 63:303–316. https://doi.org/10.1146/annurev-med-043010-193843.
21. Wagner, K., L. Unger, …, A. J. Yool. 2022. Signaling mechanisms and pharmacological modulators governing diverse aquaporin functions in hum an health and disease. *Int. J. Mol. Sci.* 23. https://doi.org/10.3390/ijms23031388.
22. Dascal, N. 2000. Voltage Clamp Recordings from Xenopus Oocytes. *Curr. Protoc. Neurosci.* 10. 6.12.1-6.12.20. https://doi.org/10.1002/0471142301.ns0612s10.
23. Campbell, E. M., D. N. Birdsell, and A. J. Yool. 2012. The activity of human aquaporin 1 as a cGMP-gated cation channel is regulated by tyrosine phosphorylation in the carboxyl-terminal domain. *Mol. Pharmacol.* 81:97–105. https://doi.org/10.1124/mol.111.073692.
24. Hazama, A., D. Kozono, …, M. Yasui. 2002. Ion permeation of AQP6 water channel protein: single-channel recordings after Hg^{2+} activation. *J. Biol. Chem.* 277:29224–29230. https://doi.org/10.1074/jbc.M204258200.
25. Byrt, C. S., M. Zhao, …, S. Tyerman. 2017. Non-selective cation channel activity of aquaporin AtPIP2;1 regulated by Ca^{2+} and pH. *Plant Cell Environ.* 40:802–815. https://doi.org/10.1111/pce.12832.
26. Kourghi, M., S. Nourmohammadi, …, A. J. Yool. 2017. Divalent cations regulate the ion conductance properties of diverse classes of aquaporins. *Int. J. Mol. Sci.* 18:2323.
27. Weber, W. M. 1999. Endogenous ion channels in oocytes of *Xenopus laevis* : recent developments. *J. Membr. Biol.* 170:1–12. https://doi.org/10.1007/s002329900532.
28. Gordon, E., T. K. Roepke, and G. W. Abbott. 2006. Endogenous KCNE subunits govern $Kv2.1K^{+}$ channel activatio n kinetics in xenopus oocyte studies. *Biophys. J.* 90:1223–1231. https://doi.org/10.1529/biophysj.105.072504.
29. Su, T. R., C. H. Chen, …, M. J. Lin. 2009. Functional study of the effect of phosphatase inhibitors on KCNQ4 channels expressed in Xenopus oocytes. *Acta Pharmacol. Sin.* 30:1220–1226. https://doi.org/10.1038/aps.2009.117.
30. Delpire, E., K. B. Gagnon, …, J. M. Wallace. 2011. Housing and husba ndry of *Xenopus laevis* affect the quality of oocytes for heterologous expression studies. *JAALAS.* 50:46–53.
31. Ehring, G. R., G. Zampighi, …, J. E. Hall. 1990. Properties of channels reconstituted from the major intrinsic protein of lens fiber membranes. *J. Gen. Physiol.* 96:631–664. https://doi.org/10.1085/jgp.96.3.631.
32. Lee, J. W., Y. Zhang, …, D. M. Roberts. 1995. Phospho rylation of nodulin 26 on serine 262 affects its voltage-sensitive channel activity in planar lipid bilayers. *J. Biol. Chem.* 270:27051–27057. https://doi.org/10.1074/jbc.270.45.27051.
33. Modesto, E., P. D. Lampe, …, A. C. Campos de Carvalho. 1996. Properties of chicken lens MIP channels reconstituted into planar lipid bilayers. *J. Membr. Biol.* 154:239–249. https://doi.org/10.1007/s002329900148.
34. Shen, L., P. Shrager, …, C. Peracchia. 1991. Cha nnel reconstitution in liposomes and planar bilayers with HPLC-purified MIP26 of bovine lens. *J. Membr. Biol.* 124:21–32. https://doi.org/10.1007/BF01871361.
35. Weaver, C. D., N. H. Shomer, …, D. M. Roberts. 1994. Nodulin 26, a nodule-specific symbiosome membrane protein from soybean, is an ion channel. *J. Biol. Chem.* 269:17858–17862. https://doi.org/10.1016/S0021-9258(17)32388-8.
36. Zampighi, G. A., J. E. Hall, and M. Kreman. 1985. Purified lens junctional prote in forms channels in planar lipid films. *Proc. Natl. Acad. Sci. USA.* 82:8468–8472. https://doi.org/10.1073/pnas.82.24.8468.
37. Saparov, S. M., D. Kozono, …, P. Pohl. 2001. Water and ion permeation of aquaporin-1 in planar lipid bilayers: Major differences in structural determinants and stoichiometry. *J. Biol. Chem.* 276:31515–31520. https://doi.org/10.1074/jbc.M104267200.
38. Henderson, S. W., S. Nourmohammadi, …, A. J. Yool. 2022. Aquaporin ion conductance properties defined by membrane environment, protein structure, and cell physiology. *Biophys. Rev.* 14:181–198. https://doi.org/10.1007/s12551-021-00925-3.
39. Salman, M. M., P. Kitchen, …, R. M. Bill. 2022. Recent breakthroughs and future directions in drugging aquaporins. *Trends Pharmacol. Sci.* 43:30–42. https://doi.org/10.1016/j.tips.2021.10.009.
40. Delcour, A. H., B. Martinac, …, C. Kung. 1989. Modified reconstitution method used in patch-clamp studies of *Escherichia coli* ion channels. *Biophys. J.* 56:631–636. https://doi.org/10.1016/S0006-3495(89)82710-9.
41. Martinac, B., P. R. Rohde, …, A. Kloda. 2010. Studying mechanosensitive ion channels using liposomes. *In* Liposomes: Methods and Protocols, Volume 2: Biological Membrane Models. V. Weissig, ed Humana Press, Totowa, NJ, pp. 31–53.
42. Matulef, K., and F. I. Valiyaveetil. 2018. Patch-clamp recordings of the KcsA K^{+} channel in unilamellar blisters. *Methods Mol. Biol.* 1684:181–191. https://doi.org/10.1007/978-1-4939-7362-0_14.

43. Nyblom, M., F. Öberg, …, K. Hedfalk. 2007. Exceptional overproduction of a functional human membrane protein. *Protein Expr. Purif.* 56:110–120. https://doi.org/10.1016/j.pep.2007.07.007.

44. Bomholt, J., C. Hélix-Nielsen, …, P. A. Pedersen. 2013. Recombinant production of human aquaporin-1 to an exceptional high membrane density in *Saccharomyces cerevisiae*. *PLoS One.* 8:e56431. https://doi.org/10.1371/journal.pone.0056431.

45. Zeder-Lutz, G., N. Cherouati, …, R. Wagner. 2006. Dot-blot immunodetection as a versatile and high-throughput assay to evaluate recombinant GPCRs produced in the yeast *Pichia pastoris*. *Protein Expr. Purif.* 50:118–127. https://doi.org/10.1016/j.pep.2006.05.017.

46. Van Sluyter, S. C., N. I. Warnock, …, E. J. Waters. 2013. Aspartic acid protease from *Botrytis cinerea* removes haze-forming proteins during white winemaking. *J. Agric. Food Chem.* 61:9705–9711. https://doi.org/10.1021/jf402762k.

47. Kourghi, M., M. L. De Ieso, …, A. J. Yool. 2018. Identification of loop D domain amino acids in the human aquaporin-1 channel involved in activation of the ionic conductance and inhibition b y AqB011. *Front. Chem.* 6:e142. https://doi.org/10.3389/fchem.2018.00142.

48. Yu, J., A. J. Yool, …, E. Tajkhorshid. 2006. Mechanism of gating and ion conductivity of a possible tetrameric pore in aquaporin-1. *Structure.* 14:1411–1423. https://doi.org/10.1016/j.str.2006.07.006.

49. Boassa, D., W. D. Stamer, and A. J. Yool. 2006. Ion channel function of aquaporin-1 natively expressed in choroid plexus. *J. Neurosci.* 26:7811–7819. https://doi.org/10.1523/jneurosci.0525-06.2006.

50. Dani, J. A. 1986. Ion-channel entrances influence permeation. Net charge, size, shape, and binding co nsiderations. *Biophys. J.* 49:607–618. https://doi.org/10.1016/S0006-3495(86)83688-8.

51. van Hoek, A. N., and A. S. Verkman. 1992. Functional reconstitution of the isolated erythroc yte water channel CHIP28. *J. Biol. Chem.* 267:18267–18269.

52. Yool, A. J., W. D. Stamer, and J. W. Regan. 1996. Forskolin stimulation of water and cation permeability in aquaporin1 water channels. *Science.* 273:1216–1218. https://doi.org/10.1126/science.273.5279.1216.

53. Tsunoda, S. P., B. Wiesner, …, P. Pohl. 2004. Aquaporin-1, nothing but a water channel. *J. Biol. Chem.* 279:11364–11367. https://doi.org/10.1074/jbc.M310881200.

54. Tong, J., J. T. Canty, …, T. J. McIntosh. 2013. The water permeability of lens aquaporin-0 depends on its lipid bilayer environment. *Exp. Eye Res.* 113:32–40. https://doi.org/10.1016/j.exer.2013.04.022.

55. Zhao, Y., A. Vararattanavech, …, C. Y. Tang. 2013. Effects of proteoliposome composition and draw solution types on separation performance of aquaporin-based proteoliposomes: implications for seawater desalination using aquaporin-based biomimetic membranes. *Environ. Sci. Technol.* 47:1496–1503. https://doi.org/10.1021/es304306t.

56. Poveda, J. A., A. M. Giudici, …, J. M. González-Ros. 2014. Lipid modulation of ion channels through specific binding sites. *Biochim. Biophys. Acta Biomembr.* 1838:1560–1567. https://doi.org/10.1016/j.bbamem.2013.10.023.

57. Tillman, T. S., and M. Cascio. 2003. Effects of membrane lipids on ion channel structure and function. *Cell Biochem. Biophys.* 38:161–190. https://doi.org/10.1385/CBB:38:2:161.

58. Nilius, B., J. Vereecke, and E. Carmeliet. 1989. Subconductance states in cardiac sodium channels. *Biomed. Biochim. Acta.* 48:S354–S357.

59. Zhang, P., Y. Luo, …, H. F. Cantiello. 2009. The multimeric structure of polycystin-2 (TRPP2): structural-functional correlates of homo- and hetero-multimers with TRPC1. *Hum. Mol. Genet.* 18:1238–1251. https://doi.org/10.1093/hmg/ddp024.

60. Kaupp, U. B., and R. Seifert. 2002. Cyclic Nucleotide-Gated Ion Channels. *Physiol. Rev.* 82:769–824. https://doi.org/10.1152/physrev.00008.2002.

61. Werten, P. J. L., L. Hasler, …, P. M. T. Deen. 2001. Large-scale purification of functional recombinant human aquaporin-2 504:200–205. https://doi.org/10.1016/S0014-5793(01)02703-X.

62. Stamer, W. D., R. W. Snyder, and J. W. Regan. 1996. Characteriza tion of the transmembrane orientation of Aquaporin-1 using antibodies to recombinant fusion proteins. *Biochemistry.* 35:16313–16318. https://doi.org/10.1021/bi9619536.

63. Kourghi, M., J. V. Pei, …, A. J. Yool. 2017. Fundamental structural and functional properties of aquaporin ion channels found across the kingdoms of life. *Clin. Exp. Pharmacol. Physiol.* https://doi.org/10.1111/1440-1681.12900.

64. Tyerman, S. D., S. A. McGaughey, …, C. S. Byrt. 2021. Adaptable and multifunctional ion-conducting aquaporins. *Annu. Rev. Plant Biol.* 72:703–736. https://doi.org/10.1146/annurev-arplant-081720-013608.

65. Ikeda, M., A. Andoo, …, K. Ishibashi. 2011. The NPC motif of aquaporin-11, unlike the NPA motif of known aquaporins, is essential for full expression of molecular fun ction. *J. Biol. Chem.* 286:3342–3350. https://doi.org/10.1074/jbc.M110.180968.

66. Itoh, T., T. Rai, …, K. Ishibashi. 2005. Identification of a novel aquaporin, AQP12, expressed in pancreatic acinar cells. *Biochem. Biophys. Res. Commun.* 330:832–838. https://doi.org/10.1016/j.bbrc.2005.03.046.

67. Pei, J. V., S. Heng, …, A. J. Yool. 2019. Development of a photoswitchable lithium-sensi ti ve probe to analyze nonselective cation channel activity in migrating cancer cells. *Mol. Pharmacol.* 95:573–583. https://doi.org/10.1124/mol.118.115428.

68. De Ieso, M. L., J. V. Pei, …, A. J. Yool. 2019. Combined pharmacological administration of AQP1 ion channel blocker AqB011 and water channel blocker Bacopaside II amplifies inhibition of colon cancer cell migration. *Sci. Rep.* 9:12635. https://doi.org/10.1038/s41598-019-49045-9.

69. Chow, P. H., C. D. Cox, …, A. J. Yool. 2022. Inhibition of the Aquaporin-1 Cation Conductance by Selected Furan Compounds Reduces Red Blood Cell Sickling. *Front. Pharmacol.* 12. https://doi.org/10.3389/fphar.2021.794791.

70. Jia, Y., Y. Zhao, …, Z. Yan. 2020. TMC1 and TMC2 proteins are pore-forming subunits of mechanosensitive ion channels. *Neuron.* 105:310–321.e3. https://doi.org/10.1016/j.neuron.2019.10.017.